On residual stresses and reference temperatures in thermo-mechanical simulations of photovoltaic modules using the finite element method

Martin Springer and Nick Bosco

***Abstract*—Thermo-mechanical simulation of photovoltaic (PV) modules using the finite element method (FEM) is a useful tool for evaluating module design features in terms of structural integrity, reliability, and durability. One of the main challenges in the numerical modeling of a PV module is the incorporation of residual stresses induced by the manufacturing process. Modeling assumptions and abstractions are necessary to limit the model complexity and reduce the computational time. However, oversimplifications and incorrect assumptions can lead to erroneous numerical results. Unfortunately, much simulation work still neglects process-induced stresses. This can lead to incorrect predictions of the stress-strain history and erroneous conclusions during the design process. Here, we review current modeling practices for incorporating process-induced stresses, and contrast numerical models that consider residual stresses with those that neglect them. We find that the simulation objective and available material properties dictate which process steps need to be modeled, and explore in depth the modeling of residual stresses induced by the lamination process. We demonstrate that a simplified cooldown procedure at the beginning of the simulation can increase the model accuracy and discuss appropriate choices for starting and reference temperatures in the finite element model.**

***Index Terms*—photovoltaic, numerical simulation, finite element method, residual stresses, thermo-mechanical**

I. Introduction

Numerical simulation tools such as the finite element method (FEM) [1] are becoming standard in the design process of new photovoltaic (PV) modules. These tools allow for the creation of physical models capable of estimating the structural behavior and degradation states of PV modules [2]. Being able to assess certain design choices early in the design process using structural mechanics simulations allows for design optimization, accelerates the development process, and can ultimately help increase the durability and reliability of the design. However, the accuracy of the numerical predictions is highly dependent on the model inputs, such as constitutive material models, boundary and loading conditions, and simplifying modeling assumptions and abstractions. A comprehensive and critical review of current FEM modeling practices for PV modules can be found in [3].

One challenge in obtaining accurate numerical results is the appropriate modeling of process-induced stresses. A simulation objective needs to be established to determine which of the stress-inducing manufacturing steps should be considered in the numerical model. Within crystalline silicon (c-Si) PV, fractured cells are one of the main degradation modes [4]. Hence, a typical simulation objective is to identify the probability of cell fracture under certain loading and environmental conditions [5], [6]. A Weibull distribution [7], [8] is commonly used to characterize the strength of PV cells; this distribution can be obtained from bare cells directly after the cutting process [9]–[11] or later in the manufacturing process—i.e., after the firing of the metallization [12], or after tabbing (application of soldered ribbon interconnects) [13]. The residual stresses and flaws induced by the manufacturing steps are reflected in the Weibull distribution at the time of characterization [14]–[16]. Thus, only stress-inducing process steps that take place after the characterization need to be considered in the numerical model. Accounting for the nucleation and growth of flaws in the numerical simulation is more challenging; hence, characterizing the fracture strength of PV cells as late as possible in the manufacturing process will deliver the most accurate results and is the preferred method for our simulation objective.

Therefore, we assume that the fracture mechanics characterization is done after the tabbing process, and the fracture mechanics analysis is carried out as explained in [5]. This way, only residual stresses from the lamination process, which induces the highest stress levels within the cells [3], [17], need to be considered in the finite element model. Modeling of the entire lamination process taking into account accurate material properties of the uncured and cured encapsulate material has not yet been accomplished, and simplifying modeling assumptions are typically used to estimate the post-lamination residual stress state [18]–[20]. Most commonly, a stress-free state is assumed at lamination temperature, and a cooldown step (to room temperature) is conducted to incorporate the residual stress state before the actual loading scenario is modeled [21]–[25]. Unfortunately, a vast proportion of simulation work is still conducted without consideration of process-induced stresses [3], leading to erroneous results.

The purpose of this work is to demonstrate the effects of neglecting the lamination-induced residual stress state on the numerical results. We assume a fracture mechanics simulation objective and use the simplified post-lamination cooldown procedure for modeling the residual stress state. This method is easy to incorporate, builds upon constitutive models of cured materials available in the literature, and increases the accuracy of the stress-strain history compared to simulations that neglect process-induced stresses. This paper provides guidance on incorporating the procedure into a finite element

Martin Springer and Nick Bosco are with the National Renewable Energy Laboratory, Golden, CO 80401 USA (e-mail: martin.springer@nrel.gov; nick.bosco@nrel.gov)

model and discusses appropriate choices for starting and reference temperatures in thermo-mechanical simulations of PV modules.

II. Method

We use a generic PV module construction with a glass front sheet and polymer backsheet for all simulations. The objective of this work is to contrast the numerical results for models containing residual stresses induced by the lamination process with the numerical results of models that neglect them. To simplify this comparison, we focus on modeling the nominal stresses in PV cells, neglecting peak stresses introduced from interconnection or mounting features. We are modeling only the PV laminate, without frame and without consideration of the interconnect technology. For a complete fracture mechanics analysis (see [5]), these features need to be incorporated into the model. Examples on how to include the interconnect technology are presented in [26], [27], and examples on how to include the frame and racking configuration are presented in [28]–[30].

A. Geometry and Material Models

We use the commercially available finite element software Ansys APDL 2020 R1 (Ansys, Inc., Canonsburg, Pennsylvania) for our simulations. We take advantage of the symmetry of a generic, 72-cell PV module and use a quarter-size model with extremely simplified boundary conditions (see Fig. 1). Symmetry boundary conditions are used along the x and y axes, and rigid body movement is prohibited by fixing the z-displacement at the top corner node of the glass front sheet.

The outside dimensions of the generic PV laminate are $995 \times 1950\,\mathrm{mm}$. Silicon cells have a size of $156 \times 156 \times 0.170\,\mathrm{mm}$ and are spaced with a $1.25\,\mathrm{mm}$ gap. The laminate consists of a $3.2\,\mathrm{mm}$-thick glass front sheet, a $0.9\,\mathrm{mm}$-thick encapsulate layer made of ethylene-vinyl acetate (EVA), and a $0.35\,\mathrm{mm}$-thick multilayer backsheet. The backsheet material consists of a poly(ethylene-terephthalate) core, with one side clad in a poly(vinyl fluoride) (PVF) and the other in poly(vinylidene fluoride), which we refer to as TPT. The multilayer backsheet was approximated by a single layer with a thickness of $0.35\,\mathrm{mm}$ and homogenized material properties.

We used linear elastic material properties for the glass front sheet (Young's Modulus, $E = 73.1\,\mathrm{GPa}$, Poisson's ratios, $\nu = 0.17$, and coefficient of thermal expansion, CTE = $9.0 \cdot 10^{-6}$ K^{-1}) as well as for the silicon cells ($E = 170\,\mathrm{GPa}, \nu = 0.28$, CTE = $2.6 \cdot 10^{-6}$ K^{-1}) [29], [31]. The latter are averaged values suitable for modeling multi-crystalline silicon cells. Temperature-dependent, linear viscoelastic material models were used for the encapsulate (EVA-T) and backsheet (TPT) [32]. The constitutive modeling was done with a Generalized Maxwell model [33] in combination with the Williams-Landel-Ferry shift function [34]. Polynomial fits of the temperature-dependent secant CTE were utilized for modeling thermal elongation [32].

We created a 3D structured mesh of the geometry with linearly interpolated continuum elements. First, the silicon cells were discretized. Four elements were used over the thickness of the silicon cells. The corner elements had element edge lengths of $1.25 \times 1.25 \times 0.0425\,\mathrm{mm}$. The planar mesh was coarsened toward the center of the cell to reduce computational time. The structured mesh was kept for all layers of the laminate, with two elements per thickness for the backsheet, the bottom and top encapsulate layer, and three elements per thickness for the glass front sheet. A mesh convergence study has been conducted, and this discretization was chosen as a good trade-off between computational time and accuracy. The chosen modeling approach resulted in approximately 1.5 million degrees of freedom.

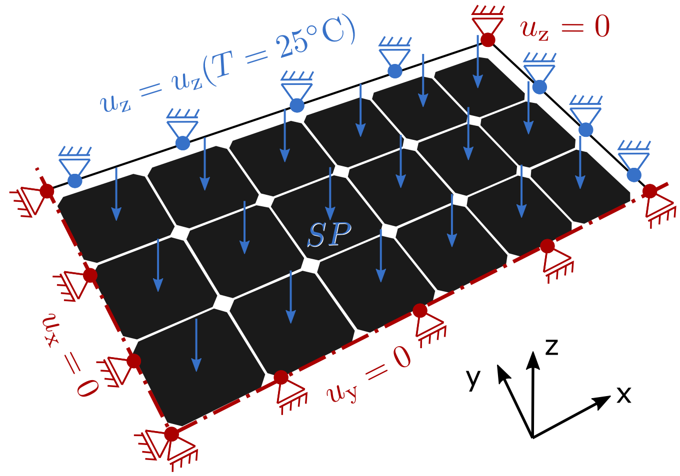

Fig. 1. Illustration of the quarter-size, structural mechanics finite element model with simplified boundary and loading conditions. Only the PV laminate, without frame and interconnections, is modeled in this work. For all load cases, symmetry boundary conditions are employed along the x and y axes, and rigid body movement is prohibited by fixing the top corner node of the glass front sheet (indicated in red). For the uniform pressure load case, the outside edges of the PV laminate are fixed along the z-axis after the cooldown step ($T = 25\,°\mathrm{C}$) and the surface pressure (SP) is applied to the glass front sheet (indicated in blue).

B. Load Cases and Reference Temperatures

We selected three typical loading scenarios relevant to PV applications (see Fig. 2). The load cases consist of static mechanical loading via the application of (i) uniform pressure loading at room temperature, (ii) an accelerated thermal cycling scenario, and (iii) a fictitious long-term relaxation situation with exposure of the module to room temperature and elevated temperatures. As outlined above, we assume that all process-induced stresses up to the tabbing step are accounted for through the experimental fracture mechanics characterization of the cells. Therefore, the only remaining process step that induces residual stresses is the PV module lamination. We incorporate the residual stresses from the lamination process through a simplified cooldown procedure at the beginning of each simulation. We assume that the starting temperature at the beginning of the cooldown step equals the reference temperature for thermal strain computations. This way, the simulation is started in a stress-free state, and the subsequent modeling steps contribute to the stress-strain history of the PV module.

We chose a set of three different reference temperatures for our study: $T_{\mathrm{ref}} = [25, 85, 145]°\mathrm{C}$. This choice is motivated by

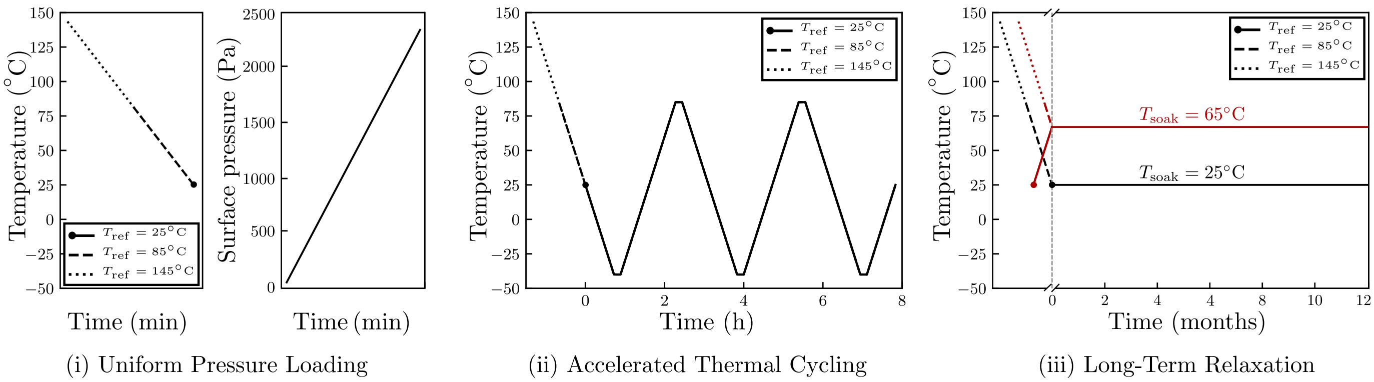

Fig. 2. Illustration of typical PV module loading scenarios. Load case (i) depicts static mechanical loading via uniform pressure loading on the glass sheet side. Prior to the mechanical loading step, a cooldown step from three different reference temperatures to room temperature (25 °C) is carried out, modeling the post-lamination residual stress state. The same cooldown procedure is used for the remaining load cases. Load case (ii) shows an accelerated thermal cycling scenario, and load case (iii) is a fictitious long-term relaxation of a PV module over the course of 1 year at two different temperature levels.

cases found in the literature for conducting thermo-mechanical simulations of PV modules. The room temperature choice, 25 °C, represents the case in which the residual stresses from the lamination process are neglected. The 85 °C choice is motivated by one of our previous works [35], where we employed a minimum energy approach to determine an appropriate stress-free temperature for a shingled cell PV model. We found that choosing a temperature close to the maximum temperature of the simulated thermal cycle presented a good approximation for the stress-free state of the module during accelerated thermal cycling. Lastly, we assumed that for the generic PV module used in this work, the highest uniform temperature during the lamination process equaled 145 °C. Using the highest lamination temperature is a popular choice for incorporating residual stresses via the simplified post-lamination cooldown procedure [3].

We simplified our model by neglecting temperature gradients, and assumed a uniform temperature distribution throughout the PV laminate. The cooldown step is carried out at a constant rate of 1.5 °C/min before each load case simulation. The static mechanical load case (i) with uniform pressure loading is conducted at room temperature (25 °C). The surface pressure is linearly ramped up to 2400 Pa over the course of 1 min. The accelerated thermal cycling load case (ii) is consistent with the procedure dictated by IEC 61215: 85 °C to −40 °C with symmetric 10 min dwell times and 1.5 °C/min ramp rates. We simulated a total of two thermal cycles and stopped the simulations at room temperature. The long-term relaxation load case (iii) simulates the relaxation behavior of the polymer materials inside the PV laminate over the course of 1 year. The motivation for this load case was to answer the question of whether residual stresses from the manufacturing process decline during the operation of the PV module. Therefore, two different soak temperatures were chosen: room temperature (25 °C), and an elevated temperature of 65 °C. The uniform module temperature is ramped from the reference temperatures to the soak temperatures at a rate of 1.5 °C/min, resulting in six individual simulations for this loading scenario.

III. RESULTS

For a fracture mechanics analysis of silicon cells, the metric of interest to assess crack initiation and propagation is the maximum tensile stress within the cells; this is best described by the first principal stress. However, the direction of the first principal stress can change during a loading scenario, and complicates the comparison of the different reference temperature simulations. Therefore, for the purpose of this work, we decided to use the σ_{yy} component of the stress tensor for easier comparison of the individual results. σ_{yy} represents the maximum tensile stress component at the end of load case (i) and is roughly equal to the first principal stress at the end of this simulation, making it a perfect candidate for our comparisons. A qualitative contour plot of the σ_{yy} distribution for load case (i), subjected to maximum surface pressure, is shown in Fig. 3. The simplified boundary conditions lead to the occurrence of nominal, maximum tensile stresses in the center cells of the model. In the following sections, all σ_{yy} results are extracted from the center of the cell, closest to the x and y symmetry condition (denoted "max" in Fig. 3).

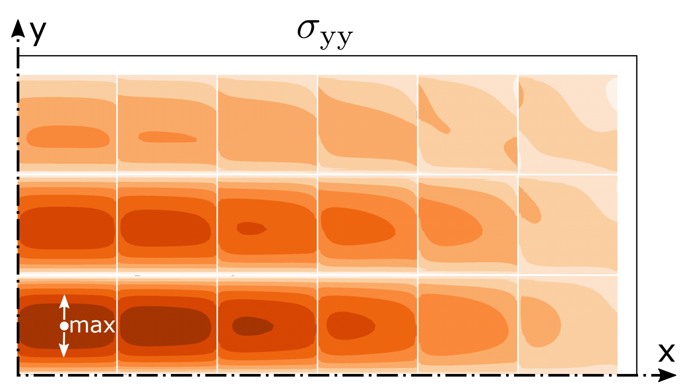

Fig. 3. Qualitative contour plot of the stress component, σ_{yy}, at 2400 Pa pressure loading. Dark colors indicate regions of high tensile stress. All subsequent results are extracted from the "max" location indicated in this figure.

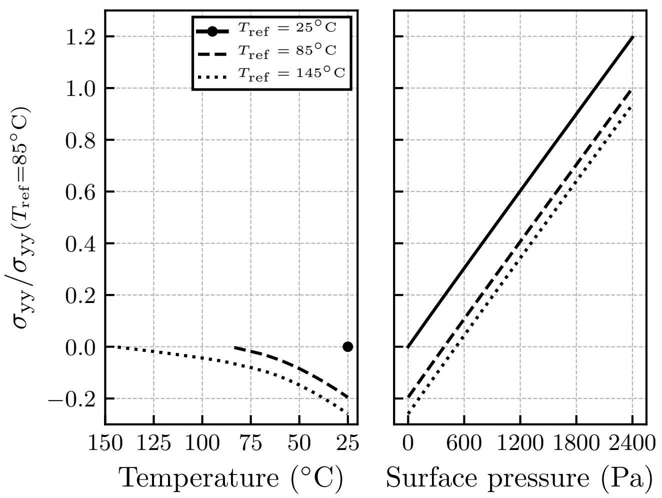

Fig. 4. Normalized σ_{yy} vs. temperature and surface pressure of the uniform pressure load case (i) at max location (Fig. 3). The left-hand side of the figure demonstrates the cooldown procedure from the three reference temperatures. The mechanical load step (right) is carried out at room temperature. This step shows a linear increase of σ_{yy} with increasing surface pressure and a constant offset between the different simulations.

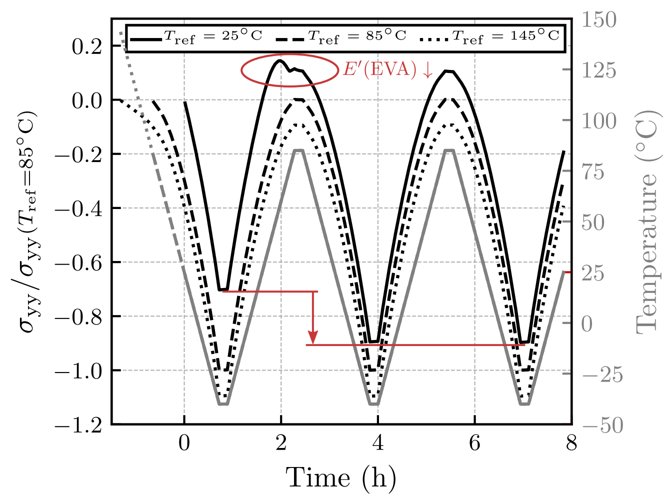

Fig. 5. Normalized σ_{yy} vs. time of accelerated thermal cycling load case (ii) at max location (Fig. 3). Prior to the two simulated accelerated thermal cycles ($t < 0\,\mathrm{h}$), the cooldown step is carried out for simulations using reference temperatures 85 °C and 145 °C. A drop in the predicted stress state between the first and second thermal cycle is visible for the simulation that neglects the residual stress state from the lamination process ($T_{\mathrm{ref}} = 25\,°\mathrm{C}$). Afterward, however, the numerical results of the different reference temperature simulations are in relatively good agreement with one another.

A. Uniform Pressure Loading

The uniform pressure load case (i) consists of two steps: a cooldown step from the reference temperature, and a mechanical loading step with increasing surface pressure (Fig. 4). All results are normalized to the final σ_{yy} value after the mechanical loading step for the simulation, with an 85 °C reference temperature. For the 25 °C reference temperature, no cooling is necessary, because the mechanical loading step is carried out at the same temperature. For simulations with higher reference temperatures, the higher CTE of the encapsulate (compared to the glass front sheet and silicon cells) leads to compressive stresses in the cells after the cooldown step. These compressive stresses are an approximation of the residual stress state induced by the lamination process. The subsequent uniform pressure loading induces tensile stresses in cells, but the initial offset between simulations starting from different reference temperatures remains constant. Although the simulation that neglects the residual stress state ($T_{\mathrm{ref}} = 25\,°\mathrm{C}$) results in 20% higher tensile stresses compared to the 85 °C reference temperature simulation, there is only a small difference (6%) in the predicted stresses between the 85 °C and 145 °C reference temperature simulations. Hence, neglecting the residual stress state for this load case scenario results in an overprediction of the tensile stresses in the silicon cells.

B. Accelerated Thermal Cycling

The accelerated thermal cycling load case (ii) starts from the three chosen reference temperatures and simulates two thermal cycles (Fig. 5). All results are normalized to the highest compressive σ_{yy} value, which occurs at the coldest temperature of $-40\,°\mathrm{C}$, for the simulation using an 85 °C reference temperature. The time axis of the results is aligned in such a way that at time $t = 0\,\mathrm{h}$, all three models are subjected to a uniform temperature of 25 °C. For the stress-free simulation, which neglects the residual stress state ($T_{\mathrm{ref}} = 25\,°\mathrm{C}$), this is equal to the starting point of the simulation. For the simulations with higher reference temperatures, the initial cooling step is done prior, and similarly to load case (i), a compressive stress state is induced into the silicon cells. For the 85 °C and 145 °C reference temperature simulations, the stresses in cycles one and two are in good agreement; σ_{yy} at the beginning of the thermal cycle ($t = 0\,\mathrm{h}$) is approximately equal to σ_{yy} at the end of the second thermal cycle. By contrast, σ_{yy} drops significantly for the 25 °C reference temperature simulation between the first and second cycle. However, after this drop, the results of all three simulations are in good agreement and differ by only $\pm 10\%$. An explanation for the drop in σ_{yy} is provided in Section IV.

C. Long-Term Relaxation

The long-term relaxation load case (iii) consists of a cooling/heating step followed by the simulation of relaxation over the course of 1 year (Fig. 6). Six individual simulations are carried out (for the three reference temperatures and two soak temperatures). All results are normalized to the final σ_{yy} value of the simulation utilizing the 85 °C reference temperature and a soak temperature of 25 °C. The residual stress buildup from the post-lamination cooling step is visible at $t = 0$. For simulations with a reference temperature that is higher than the soak temperature, a compressive stress state is obtained, whereas for the simulation that neglects the residual stresses ($T_{\mathrm{ref}} = 25\,°\mathrm{C}$) and has a soak temperature of 65 °C, a tensile stress state is obtained. In the latter case, a significant amount of relaxation can be observed by the rapid decline of σ_{yy} values directly after the heating step. In the other simulations, a more moderate decline in σ_{yy} can be observed. In general, relaxation occurs at a faster rate for simulations with a higher soak

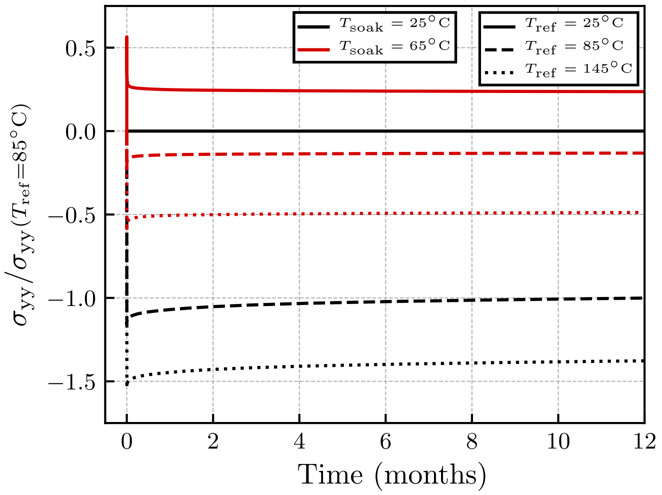

Fig. 6. Normalized σ_{yy} vs. time for long-term relaxation load case (iii) at max location (Fig. 3). The six different simulations are cooled/heated from the reference temperature to the soak temperatures, leading to either compressive or tensile stresses in the silicon cells ($t = 0\,\mathrm{h}$). Subsequently, the viscoelastic relaxation of the polymer materials inside the PV module leads to a declining stress state in the silicon cells over the simulation time of 1 year.

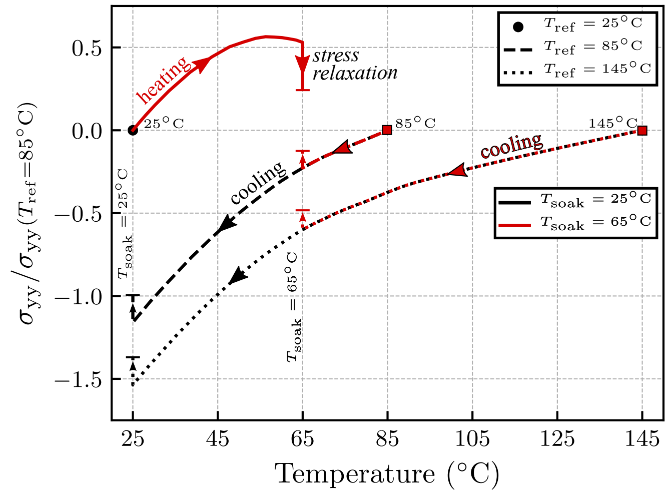

Fig. 7. Normalized σ_{yy} vs. temperature for long-term relaxation load case (iii) at max location (Fig. 3). The six different simulations are cooled/heated from the reference temperature to the soak temperatures. Subsequently, the viscoelastic relaxation of the polymer materials leads to a declining stress state, which is depicted by the vertical lines at the soak temperatures.

temperature ($65\,°\mathrm{C}$). For simulations with a soak temperature of $25\,°\mathrm{C}$, a steady decline in σ_{yy} can be observed up to roughly eight months after the start of the simulations. Afterward, the stress state remains almost constant.

An alternative way of presenting these results is to plot the stress evolution over temperature instead of time (Fig. 7). Here, the impact of the temperature change on the stress evolution is easier to visualize, and the stress relaxation is depicted by the vertical decline in the stress states. For all simulations, stresses induced due to temperature changes are larger than the stress relaxation caused by the viscoelastic material response.

IV. Discussion

Understanding the constitutive behavior of the encapsulate material is key to interpreting the presented results. As outlined above, we used a temperature-dependent, linear, viscoelastic material model to describe the constitutive behavior of the EVA encapsulate [32]. We have chosen EVA because it is the dominant encapsulate material by world market share at the time of writing and is predicted to remain the dominant choice in the coming years [36]. The discussion here is focused on EVA and other materials can induce different residual stress states after lamination. However, for materials with similar mechanical properties (e.g., polyolefin (see [32])) comparable residual stress states and conclusions on reference temperatures are expected.

The temperature- and loading-rate-dependent storage modulus, E', of EVA predicted by a Generalized Maxwell model, is shown in Fig. 8. In a previous work [37], we identified the relevant loading frequency range for PV applications as $3 \cdot 10^{-8}\,\mathrm{Hz}$ to $100\,\mathrm{Hz}$, to account for loading scenarios from seasonal temperature changes and vibrations causing first- and second-harmonic resonance frequencies, respectively. Also depicted is a loading frequency of $1 \cdot 10^{-4}\,\mathrm{Hz}$, which roughly approximates the storage modulus for the accelerated thermal cycling simulation and the cooldown steps. By contrast, the $1\,\mathrm{Hz}$ curve of the storage modulus is more closely related to the surface pressure loading step in load case (i).

Noticeably, our material model levels out at $\approx 0.75\,\mathrm{MPa}$. This is because the materials characterization has been conducted up to $95\,°\mathrm{C}$ in [32], which is sufficient to capture the normal operating temperature range for PV modules. However, for accurately modeling the lamination process, materials characterizations at higher temperatures would be required. Other groups have reported dynamic mechanical analysis (DMA) results of EVA measurements for temperatures up to $150\,°\mathrm{C}$ [20], [21], which show a similar plateau as our numerical model. We believe that the accuracy limits of the DMA have been reached in those studies and the reported storage modulus values may have a high level of uncertainty at such elevated temperatures. Either way, all the aforementioned studies show that the storage modulus of EVA above $95\,°\mathrm{C}$ is below $1\,\mathrm{MPa}$, which indicates that the encapsulate has practically lost its structural integrity to transfer relevant levels of shear stresses for engineering applications. From a numerical modeling perspective, this plateau means that the temperature-dependent, linear, viscoelastic material model is reduced to a single storage modulus value, comparable to a linear elastic material model.

The accuracy of the modeled residual stress state from the lamination process is dependent on how accurately the material model describes the structural behavior of the encapsulate at those elevated temperatures. Our model predicts constant values for temperatures above $95\,°\mathrm{C}$, whereas a further decline would be expected. However, since the structural integrity of the encapsulate material is practically lost, the differences in the stress states between the model predictions and the actual material response will be negligible small. This can be seen in our load case (i) simulations (Fig. 4). There, the

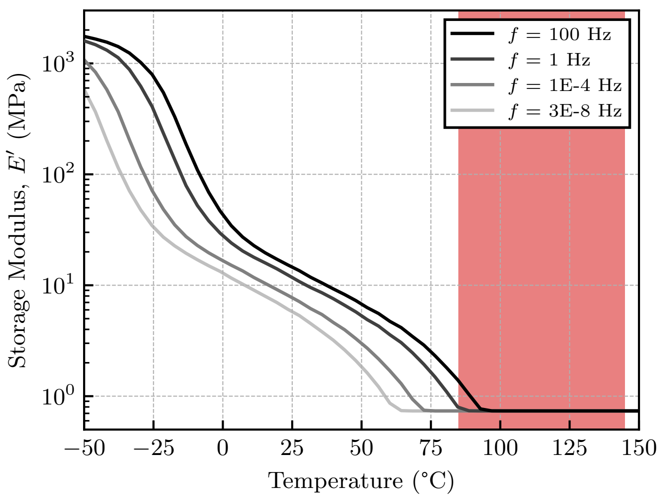

Fig. 8. Temperature- and rate-dependent storage modulus of the EVA encapsulate material, predicted by a Generalized Maxwell model [32]. The viscoelastic constitutive model collapses to a single storage modulus value ($\approx 0.75\,\mathrm{MPa}$) at elevated temperatures, where most of the structural integrity of the material is lost. The filled region indicates our choices for starting and reference temperatures ($T_{\mathrm{ref}} = 85\,°\mathrm{C}$ to $145\,°\mathrm{C}$) for simulations, considering the residual stresses induced by the lamination process.

discrepancy between the simulations using either $T_{\mathrm{ref}} = 145\,°\mathrm{C}$ or $T_{\mathrm{ref}} = 85\,°\mathrm{C}$ as reference temperature resulted in only a 6% difference in the predicted tensile stresses, which should be sufficiently accurate for most engineering tasks. Assuming that our numerical model overpredicts the storage modulus at elevated temperatures, this difference will be even smaller once higher-accuracy material models become available. Further, this results indicate that a wide range of applicable reference temperatures are suitable to predict the residual stress state from the lamination step reasonable well. By contrast, the simulation that neglected the residual stress state resulted in a 20% to 26% higher tensile stress state. Therefore, simulations that are neglecting the residual stress state are likely to overpredict the probability of cell fracture.

Similar considerations can be made for load case (ii), where higher reference temperatures lead to higher compressive stresses in the silicon cells during accelerated thermal cycling (Fig. 5). After the first thermal cycle, the predicted stress states between the different reference temperature simulations differ by only $\pm 10\%$. The most interesting feature of these simulations is the drop in σ_{yy} between the first and second thermal cycle for the simulation that neglects the residual stress state. The assumption of a stress-free state at the beginning of this simulation is clearly inaccurate, but heating the module to elevated temperatures leads to a "self-correcting" behavior in the simulation. The compliance of the encapsulate material increases significantly at elevated temperatures and leads to a decline of the storage modulus, E' (Fig. 8). At around $55\,°\mathrm{C}$ the stress reduction (caused by the decrease in E' and viscoelastic relaxation) exceeds the stress built-up during heating (caused by the mismatch in CTE of the involved materials), leading to a drop in the tensile stress state, as indicated by the red circle in Fig. 5. At such elevated temperatures, the encapsulate is not capable of transferring high enough shear stresses from the glass front sheet to the silicon cells. Hence, the unphysical assumption of a stress-free state is "corrected" during the first heating cycle, resulting in a more appropriate prediction of the actual stress state in the second thermal cycle. How well this model will predict the actual stress state depends on the maximum temperature of the heating cycle and, again, the accuracy of the constitutive model at elevated temperatures. Additionally, this simulation shows that the assumption of a stress-free state of the encapsulate material at lamination temperature may be reasonable, because even at a temperature lower than the lamination temperature, the encapsulate material fails to transfer a significant amount of shear stresses from the glass front sheet to the silicon cells.

A similar behavior can be observed in the load case (iii) simulations (Fig. 6 and Fig. 7). Here, the model that neglects the residual stress state ($T_{\mathrm{ref}} = 25\,°\mathrm{C}$ and $T_{\mathrm{soak}} = 65\,°\mathrm{C}$) is carrying out a similar "self-correcting" step when heated to the soak temperature. At elevated temperatures of around $55\,°\mathrm{C}$, the encapsulate fails to transfer shear stresses from the front sheet to the silicon cells. Additionally, viscoelastic relaxation leads to a significant drop of the stresses at the beginning of the soaking step. In contrast, simulations that consider residual stresses result in a much more moderate decline of the stress state during long-term exposure. Further, the simulated time frame of 1 year showed that stress relaxation slows over time with a residual stress state remaining in the model. These results indicate that, even for long-term exposure at elevated temperatures, the residual stresses induced by the lamination process do not vanish over time, and will impact the stress-strain history of the PV laminate over the course of its lifetime.

V. Conclusion

We explored three typical loading scenarios of PV modules using models that considered and neglected the residual stress state after lamination. We found that incorporating process-induced stresses is especially important for mechanical loading scenarios, where neglecting the residual stresses led to differences of up to 26% in the stress states. In contrast, all models subjected to accelerated thermal cycling conditions showed better agreement of the predicted stress states after the first thermal cycle. This is because the encapsulate material becomes compliant at elevated temperatures and cannot transfer a significant amount of shear stresses from the front sheet to the cells, which justifies the common assumption of a stress-free state at lamination temperature. Lastly, the simulations that modeled long-term relaxation of PV modules showed that the post-lamination residual stresses do not significantly decline over time, even at elevated temperatures. Hence, process-induced stresses affect the whole stress-strain history of a PV module over its lifetime and need to be considered in numerical models. Ultimately, the accuracy of the encapsulate material model at elevated temperatures will define the accuracy of the predicted residual stress state after lamination. However, we have shown that, for currently available constitutive models of EVA, a wide range of starting and reference temperatures ($85\,°\mathrm{C}$ to $145\,°\mathrm{C}$) resulted in similar predictions of the stress and strain history. Thus, for module designs using EVA or encapsulates with similar mechanical properties, a simplified cooldown procedure at the beginning of the simulation should be sufficiently accurate for most engineering tasks, and we recommend incorporating this procedure into thermo-mechanical simulations of PV modules.

VI. Acknowledgment

This work was authored by the National Renewable Energy Laboratory, operated by Alliance for Sustainable Energy, LLC, for the U.S. Department of Energy (DOE) under Contract No. DE-AC36-08GO28308. Funding provided as part of the Durable Modules Consortium (DuraMAT), an Energy Materials Network Consortium funded by the U.S. Department of Energy, Office of Energy Efficiency and Renewable Energy, Solar Energy Technologies Office. The views expressed in the article do not necessarily represent the views of the DOE or the U.S. Government. The U.S. Government retains and the publisher, by accepting the article for publication, acknowledges that the U.S. Government retains a nonexclusive, paid-up, irrevocable, worldwide license to publish or reproduce the published form of this work, or allow others to do so, for U.S. Government purposes.

References

[1] J. N. Reddy, *Introduction to the Finite Element Method, Fourth Edition*. McGraw-Hill Education, 2019. [Online]. Available: https://www.accessengineeringlibrary.com/content/book/9781259861901

[2] M. Springer and N. Bosco, "Environmental influence on cracking and debonding of electrically conductive adhesives," *Engineering Fracture Mechanics*, vol. 241, p. 107398, Jan. 2021. [Online]. Available: https://www.sciencedirect.com/science/article/pii/S0013794420309760

[3] P. Nivelle, J. A. Tsanakas, J. Poortmans, and M. Daenen, "Stress and strain within photovoltaic modules using the finite element method: A critical review," *Renewable and Sustainable Energy Reviews*, vol. 145, p. 111022, Jul. 2021. [Online]. Available: https://www.sciencedirect.com/science/article/pii/S1364032121003129

[4] D. C. Jordan, T. J. Silverman, J. H. Wohlgemuth, S. R. Kurtz, and K. T. VanSant, "Photovoltaic failure and degradation modes," *Progress in Photovoltaics: Research and Applications*, vol. 25, no. 4, pp. 318–326, 2017, _eprint: https://onlinelibrary.wiley.com/doi/pdf/10.1002/pip.2866. [Online]. Available: https://onlinelibrary.wiley.com/doi/abs/10.1002/pip.2866

[5] N. Bosco, M. Springer, J. Liu, S. Nalin Venkat, and R. H. French, "Employing Weibull Analysis and Weakest Link Theory to Resolve Crystalline Silicon PV Cell Strength Between Bare Cells and Reduced- and Full-Sized Modules," *IEEE Journal of Photovoltaics*, vol. 11, no. 3, pp. 731–741, May 2021, conference Name: IEEE Journal of Photovoltaics.

[6] M. Sander, S. Dietrich, M. Pander, M. Ebert, and J. Bagdahn, "Systematic investigation of cracks in encapsulated solar cells after mechanical loading," *Solar Energy Materials and Solar Cells*, vol. 111, pp. 82–89, Apr. 2013. [Online]. Available: https://www.sciencedirect.com/science/article/pii/S0927024812005612

[7] W. Weibull, "A statistical theory of strength of materials," *Ingenioersvetenskapsakad.-Handl.*, vol. 151, p. 45 pp., 1939.

[8] F. W. Zok, "On weakest link theory and Weibull statistics," *Journal of the American Ceramic Society*, vol. 100, no. 4, pp. 1265–1268, Apr. 2017. [Online]. Available: https://onlinelibrary.wiley.com/doi/10.1111/jace.14665

[9] O. Borrero-López, T. Vodenitcharova, M. Hoffman, and A. J. Leo, "Fracture Strength of Polycrystalline Silicon Wafers for the Photovoltaic Industry," *Journal of the American Ceramic Society*, vol. 92, no. 11, pp. 2713–2717, 2009, _eprint: https://ceramics.onlinelibrary.wiley.com/doi/pdf/10.1111/j.1551-2916.2009.03287.x. [Online]. Available: https://ceramics.onlinelibrary.wiley.com/doi/abs/10.1111/j.1551-2916.2009.03287.x

[10] L. Zhao, D. Nelias, D. Bardel, A. Maynadier, P. Chaudet, and B. Marie, "On the fracture of multi-crystalline silicon wafer," *Journal of Physics D: Applied Physics*, vol. 49, no. 47, p. 475601, Nov. 2016, publisher: IOP Publishing. [Online]. Available: https://doi.org/10.1088/0022-3727/49/47/475601

[11] F. Kaule, M. Pander, M. Turek, M. Grimm, E. Hofmueller, and S. Schoenfelder, "Mechanical damage of half-cell cutting technologies in solar cells and module laminates," *AIP Conference Proceedings*, vol. 1999, no. 1, p. 020013, Aug. 2018, publisher: American Institute of Physics. [Online]. Available: https://aip.scitation.org/doi/10.1063/1.5049252

[12] S. Schoenfelder, S. Meyer, and F. Kaule, "Benchmarking Mechanical Strength Data for New Solar Cell Concepts," *33rd European Photovoltaic Solar Energy Conference and Exhibition*, pp. 276–279, Nov. 2017, iSBN: 9783936338478 Publisher: WIP. [Online]. Available: http://www.eupvsec-proceedings.com/proceedings?paper=42108

[13] M. W. Rowell, S. G. Daroczi, D. W. J. Harwood, and A. M. Gabor, "The Effect of Laminate Construction and Temperature Cycling on the Fracture Strength and Performance of Encapsulated Solar Cells," in *2018 IEEE 7th World Conference on Photovoltaic Energy Conversion (WCPEC) (A Joint Conference of 45th IEEE PVSC, 28th PVSEC 34th EU PVSEC)*, Jun. 2018, pp. 3927–3931, iSSN: 0160-8371.

[14] R. Samuel, S. Chandrasekar, T. N. Farris, and R. H. Licht, "Effect of Residual Stresses on the Fracture of Ground Ceramics," *Journal of the American Ceramic Society*, vol. 72, no. 10, pp. 1960–1966, 1989, _eprint: https://ceramics.onlinelibrary.wiley.com/doi/pdf/10.1111/j.1151-2916.1989.tb06007.x. [Online]. Available: https://ceramics.onlinelibrary.wiley.com/doi/abs/10.1111/j.1151-2916.1989.tb06007.x

[15] C. Funke, E. Kullig, M. Kuna, and H. J. Möller, "Biaxial Fracture Test of Silicon Wafers," *Advanced Engineering Materials*, vol. 6, no. 7, pp. 594–598, 2004, _eprint: https://onlinelibrary.wiley.com/doi/pdf/10.1002/adem.200400406. [Online]. Available: https://onlinelibrary.wiley.com/doi/abs/10.1002/adem.200400406

[16] C. Yang, F. Mess, K. Skenes, S. Melkote, and S. Danyluk, "On the residual stress and fracture strength of crystalline silicon wafers," *Applied Physics Letters*, vol. 102, no. 2, p. 021909, Jan. 2013, publisher: American Institute of Physics. [Online]. Available: https://aip.scitation.org/doi/10.1063/1.4776706

[17] A. J. Beinert, P. Romer, A. Büchler, V. Haueisen, J. Aktaa, and U. Eitner, "Thermomechanical stress analysis of PV module production processes by Raman spectroscopy and FEM simulation," *Energy Procedia*, vol. 124, pp. 464–469, Sep. 2017. [Online]. Available: https://www.sciencedirect.com/science/article/pii/S1876610217342261

[18] S.-H. Schulze, M. Pander, S. Müller, C. Ehrich, and M. Ebert, "Influence of Vacuum Lamination Process on Laminate Properties – Simulation and Test Results," in *24th European Photovoltaic Solar Energy Conference*, Hamburg, Germany, Sep. 2009, pp. 3367 – 3372.

[19] W. J. R. Song, S. K. Tippabhotla, A. A. O. Tay, and A. S. Budiman, "Numerical Simulation of the Evolution of Stress in Solar Cells During the Entire Manufacturing Cycle of a Conventional Silicon Wafer Based Photovoltaic Laminate," *IEEE Journal of Photovoltaics*, vol. 8, no. 1, pp. 210–217, Jan. 2018, conference Name: IEEE Journal of Photovoltaics.

[20] S. K. Tippabhotla, W. J. R. Song, A. A. O. Tay, and A. S. Budiman, "Effect of encapsulants on the thermomechanical residual stress in the back-contact silicon solar cells of photovoltaic modules – A constrained local curvature model," *Solar Energy*, vol. 182, pp. 134–147, Apr. 2019. [Online]. Available: https://www.sciencedirect.com/science/article/pii/S0038092X19301549

[21] S. Dietrich, M. Pander, M. Sander, S. H. Schulze, and M. Ebert, "Mechanical and thermomechanical assessment of encapsulated solar cells by finite-element-simulation," in *Reliability of Photovoltaic Cells, Modules, Components, and Systems III*, vol. 7773. International Society for Optics and Photonics, Aug. 2010, p. 77730F. [Online]. Available: https://www.spiedigitallibrary.org/conference-proceedings-of-spie/7773/77730F/Mechanical-and-thermomechanical-assessment-of-encapsulated-solar-cells-by-finite/10.1117/12.860661.short

[22] M. Gonzalez, J. Govaerts, R. Labie, I. De Wolf, and K. Baert, "Thermo-mechanical challenges of advanced solar cell modules," in *2011 12th Intl. Conf. on Thermal, Mechanical Multi-Physics Simulation and Experiments in Microelectronics and Microsystems*, Apr. 2011, pp. 1/7–7/7.

[23] U. Eitner, M. Pander, S. Kajari-Schröder, M. Köntges, and H. Altenbach, "Thermomechanics of PV Modules Including the Viscoelasticity of EVA," in *26th European Photovoltaic Solar Energy Conference and Exhibition*, 2011, pp. 3267 – 3269.

[24] S. Dietrich, M. Pander, M. Sander, and M. Ebert, "Mechanical Investigations on Metallization Layouts of Solar Cells with Respect to Module Reliability," *Energy Procedia*, vol. 38, pp. 488–497, Jan.

2013. [Online]. Available: https://www.sciencedirect.com/science/article/pii/S1876610213013945
[25] Q. Z. Zhang, B. F. Shu, M. B. Chen, Q. B. Liang, C. Fan, Z. Q. Feng, and P. J. Verlinden, “Numerical investigation on residual stress in photovoltaic laminates after lamination,” *Journal of Mechanical Science and Technology*, vol. 29, no. 2, pp. 655–662, Feb. 2015. [Online]. Available: https://doi.org/10.1007/s12206-015-0125-y
[26] P.-C. Hsiao, C. Chen, G. Chen, X. Zhang, A. Lennon, Z. Wang, N. Song, Y. Li, Z. Ouyang, C. Hall, C. Zhu, J. Lv, and C. Shen, “Comparative Models of Induced Thermomechanical Stress in Silicon Solar Cells Interconnected with Conventional Tabbing and Wire-Based Interconnection Methods,” *2019 IEEE 46th Photovoltaic Specialists Conference (PVSC)*, 2019.
[27] G. Li, M. W. Akram, Y. Jin, X. Chen, C. Zhu, A. Ahmad, R. H. Arshad, and X. Zhao, “Thermo-mechanical behavior assessment of smart wire connected and busbarPV modules during production, transportation, and subsequent field loading stages,” *Energy*, vol. 168, pp. 931–945, Feb. 2019. [Online]. Available: https://www.sciencedirect.com/science/article/pii/S0360544218323685
[28] J. Y. Hartley, A. Maes, M. Owen-Bellini, T. Truman, E. Elce, A. Ward, T. Khraishi, and S. Roberts, “Effects of Photovoltaic Module Materials and Design on Module Deformation Under Load,” in *2019 IEEE 46th Photovoltaic Specialists Conference (PVSC)*, Jun. 2019, pp. 0511–0516, iSSN: 0160-8371.
[29] J. Y. Hartley, “Effects of Frame Constraints on Internal Module Damage During Mechanical Load Testing,” in *2021 IEEE 48th Photovoltaic Specialists Conference (PVSC)*, 2021.
[30] H. Li, D. Zhang, Z. Qin, L. Li, and E. Zhang, “Analysis of Deformation and Strength of Solar Module Support under Wind-Wave Load.” Atlantis Press, Dec. 2015, pp. 1626–1629, iSSN: 2352-5401. [Online]. Available: https://www.atlantis-press.com/proceedings/icmse-15/25845821
[31] N. Bosco, T. J. Silverman, and S. Kurtz, “Climate specific thermomechanical fatigue of flat plate photovoltaic module solder joints,” *Microelectronics Reliability*, vol. 62, pp. 124–129, Jul. 2016. [Online]. Available: https://www.sciencedirect.com/science/article/pii/S0026271416300609
[32] N. Bosco, M. Springer, and X. He, “Viscoelastic Material Characterization and Modeling of Photovoltaic Module Packaging Materials for Direct Finite-Element Method Input,” *IEEE Journal of Photovoltaics*, vol. 10, no. 5, pp. 1424–1440, Sep. 2020, conference Name: IEEE Journal of Photovoltaics.
[33] H. F. Brinson and L. C. Brinson, *Polymer Engineering Science and Viscoelasticity: An Introduction*, 2nd ed. Springer US, 2015. [Online]. Available: https://www.springer.com/gp/book/9781489974846
[34] M. L. Williams, R. F. Landel, and J. D. Ferry, “The Temperature Dependence of Relaxation Mechanisms in Amorphous Polymers and Other Glass-forming Liquids,” *Journal of the American Chemical Society*, vol. 77, no. 14, pp. 3701–3707, Jul. 1955, publisher: American Chemical Society. [Online]. Available: https://doi.org/10.1021/ja01619a008
[35] M. Springer, J. Hartley, and N. Bosco, “Multiscale Modeling of Shingled Cell Photovoltaic Modules for Reliability Assessment of Electrically Conductive Adhesive Cell Interconnects,” *IEEE Journal of Photovoltaics*, vol. 11, no. 4, pp. 1040–1047, Jul. 2021, conference Name: IEEE Journal of Photovoltaics.
[36] M. Fischer, M. Woodhouse, S. Herritsch, and J. Trube, “International Technology Roadmap for Photovoltaic (ITRPV),” VDMA, Tech. Rep. 13. Edition, 2021.
[37] M. Springer and N. Bosco, “Linear viscoelastic characterization of electrically conductive adhesives used as interconnect in photovoltaic modules,” *Progress in Photovoltaics: Research and Applications*, vol. 28, no. 7, pp. 659–681, 2020. [Online]. Available: https://onlinelibrary.wiley.com/doi/abs/10.1002/pip.3257